Nanoscale

Accepted Manuscript

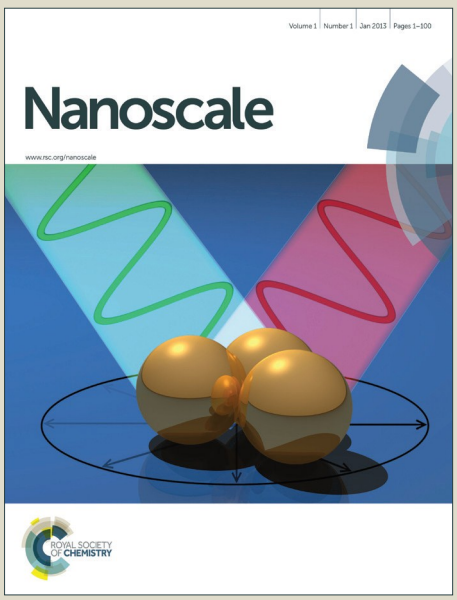

ROYAL SOCIETY OF CHEMISTRY

www.rsc.org/nanoscale

Nanoscale

ARTICLE

Broadly Tunable Graphene Plasmons Using an Ion-gel Top Gate with Low Control Voltage

Received 00th January 20xx,
Accepted 00th January 20xx

DOI: 10.1039/x0xx00000x

www.rsc.org/

Hai Hu,[a] Feng Zhai,[b] Debo Hu,[a] Zhenjun Li,[a] Bing Bai,[a] Xiaoxia Yang,*[a] and Qing Dai*[a]

The electrostatic tunability of graphene is vital for the field of active plasmons and would be beneficial in tunable infrared and Terahertz optical element applications. The key to realizing broad tunability is achieving high carrier densities in graphene. Here we use ion-gel, currently one of the most efficient dielectrics with ultra-high capacitance, to realize broadly tunable graphene plasmons (~1270 cm^{-1}) with low voltage modulation (~4 V shifted from Dirac point). We further explore the coupling between graphene plasmons and the molecular vibration modes of ion-gel, since strong plasmon-phonon coupling can split the plasmon resonance peak into multi-peaks and reduce their tunability. Our experiments demonstrate weak plasmon-phonon coupling in the graphene/ion-gel system, which has limited effects on plasmon properties. These make ion-gel an effective dielectric for broadly tunable graphene plasmonic devices, such as new optical modulators, filters and wavelength multiplexers.

Introduction

Plasmons can be used to concentrate and manipulate light at the nanoscale which is substantially below the diffraction limit. Because of this unique ability, plasmons have been applied in subwavelength optics, metamaterials and chemical and biological sensors.[1-3] While traditional plasmonic materials (e.g. gold and silver) function at visible wavelengths, graphene plasmons is more fundamentally suited to manipulate photons in communication system, security inspection and sensing applications as they can be tuned from near-infrared to terahertz.[4-7] Moreover, graphene plasmons have very low intrinsic damping rates, ultra-high electromagnetic field confinements, and a dynamic tunability which can be easily achieved by gating in an analogous manner as field effect transistors (FET).[5-9]

Based on these remarkable properties, a series of novel plasmonic devices, such as tunable modulators, [10, 11] filters, [12, 13] and detectors, [14] have been proposed recently. Development of a broadly tunable plasmonic device with low control voltage would further improve the practicability of these existing plasmonic devices. Enhancing doping efficiency and carrier density of graphene is an important approach to implement this functionality. Optimize the electronic doping design with proper dielectric materials to enhance doping efficiency and carrier density of graphene seems to be a promising approach. There are three main types of dielectric materials which are widely used in current electrical tunable graphene devices. Conventional SiO_2 dielectric is beneficial for identifying and processing graphene flakes,[15,16] but only gives graphene carrier densities on the order of 10^{13} cm^{-2}.[17-19] High-κ dielectrics (1-2 μFcm^{-2}), such as ZrO_2, Al_2O_3, and HfO_2 have also been used to obtain high doping, [20-25] but their applications have been limited due to the necessity of high growth temperatures and the complexity of processing conditions.[26] Ion-gel is one of the most efficient dielectric materials with a very high gate capacitance of about 10 μFcm^{-2}, which is ~800 times larger than the widely used 300 nm SiO_2 (12 $nFcm^{-2}$).[15, 18, 27] Ion-gel can be employed to shift the Fermi level (E_F) of graphene significantly from about -1.5 to 2.5 eV by applying a small top gate voltage (~10 V). This E_F shift corresponds to carrier densities ranging from about -1 to 2.5×10^{14} cm^{-2}.[27] Ion-gel gate dielectric materials are also transparent, and have good mechanical flexibility, fatigue stability, as well as excellent electrochemical and thermal stability,[28-30] which makes them compatible with tunable graphene plasmonic devices on varied substrates, such as SiO_2[12,31] and In_2O_3/BaF_2[32]. F. Wang's group reported tunable terahertz graphene plasmonics from about 60 to 200 cm^{-1}. However, the tunability of graphene plasmons in the mid-IR spectrum range and the influence of ion-gel phonon on them are still unclear. The plasmon-phonon coupling can change graphene plasmon significantly, such as their dispersion, tunability and lifetime, thus studying the plasmonic of graphene/ion-gel system in mid-IR is of fundamental importance. For example, the strong plasmon-phonon couplings in graphene/SiO_2 and grapheme/*h*-BN systems split the plasmon resonance peak into multi-peaks and dramatically change their frequencies, tunability and lifetimes.[33]

[a] National Center for Nanoscience and technology, Beijing 100190, China. E-mail: daiq@nanoctr.cn, yangxx@nanoctr.cn ;Tel: +86-010-82545720
[b] Department of Physics, Zhejiang Normal University, Jinhua 321004, China.
† Electronic Supplementary Information (ESI) available: [details of any supplementary information available should be included here]. See DOI: 10.1039/x0xx00000x

In this work, a broadly tunable graphene plasmon of ~1242 cm^{-1} shifting (corresponding to ~0.88 eV shifting of E_F) was realized through a low voltage modulation (4 V shifting from Dirac point) by using a conveniently spin-coated ion-gel thin film. In contrast, the SiO_2 back gate led to 379 cm^{-1} shifting with nearly 200 V gate voltage modulation on the same device. We further explored the coupling between graphene plasmons and the molecular vibration modes of ion-gel, since strong plasmon-phonon coupling can split the plasmon resonance peak into multi-peaks and reduce their tunability. Our experiments demonstrate weak plasmon-phonon coupling in the graphene/ion-gel system. Our results also show that ion-gel has limited effects on graphene plasmon lifetimes. These results indicate that ion-gel thin film is an effective dielectric for broadly tunable graphene plasmon devices with limited phonon-plasmon coupling influence.

Results and Discussion

Device Fabrication and Experimental Set-up

Graphene nanoribbon arrays were used to excite localized graphene plasmons. Figure 1a shows a schematic view of the measurement set-up. First, a graphene sheet was transferred onto a SiO_2/Si substrate and then patterned into electrically continuous nanoribbon arrays with a gap-to-width ratio of 1:1 (Figure 1b). Two Cr/Au electrodes were deposited on the graphene for electrical characterization and a third one was deposited on the outside of the graphene as an in-plane top-gate electrode (Figure 1b). This design is used to avoid metal atoms penetrating into the ion-gel film which can occur when the top electrode is made by evaporating and to prevent external contamination.[34] A film of ion-gel was spin coated onto the device as the top-gate dielectric while a SiO_2 film was used as the back-gate dielectric with highly doped Si as the back gate.

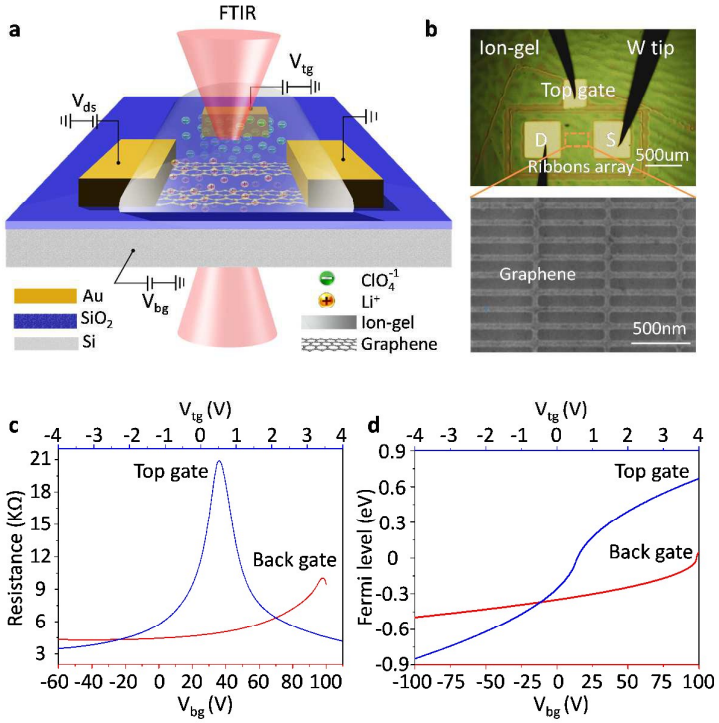

Figure 1. (a) Schematic of the experiment for measuring extinction spectra of the ion-gel top-gated graphene nanoribbon array by FTIR microscopy. Highly doped Si and SiO_2 were used as back gate and dielectric in the same device for comparison. (b) Top: Optical micrograph of a fabricated device coated with ion-gel film (green waves). Bottom: Scanning electron microscopy (SEM) image of a graphene nanoribbon array with a ribbon width of ~65 nm and a gap-to-ribbon ratio of 1:1. (c) Representative transfer characteristics of the device controlled by the top gate voltage V_{tg} (blue curve) and the back gate voltage V_{bg} (red curve), respectively. (d) The dependence of the graphene Fermi levels on V_{tg} and V_{bg}, respectively.

Using ion-gel top gate can shift the Fermi level of graphene in a wide range with small gate voltages because of the high capacitance of ion-gel. This high capacitance results from the nanometer thick (1-5 nm) Debye layer formed at the ion-gel/graphene interface.[35-38] As illustrated in Figure 1a, with a positive gate bias, negative ions (ClO_4^-) in the ion-gel move toward and accumulate near the top-gate electrode while positive ions (Li^+) accumulate on the surface of the graphene channel. The accumulated Li^+ ions create a positive electric field, which draws electrons into the graphene channel. When a negative voltage is applied, holes are injected into graphene. Thus, by using ion-gel top gate, we were able to obtain highly doped graphene nanoribbons with actively tunable carrier densities via small gate voltages. In addition, the applied gate voltages should be limited in the range from -5 to 5 V in order to prevent unwanted chemical reactions.[39]

The plasmonic properties of graphene at different Fermi levels E_F were characterized by using a Fourier transform

infrared microscopy (FTIR). First, the extinction spectra (T(*CNP*)) of the graphene nanoribbon array at the charge neutral point (CNP) (i.e. E_F=0) were detected. Then we changed E_F of the graphene nanoribbon array, and measured its extinction spectra T(E_F). The electromagnetic response of the graphene plasmon at E_F was obtained from the extinction spectrum T, where T=*1*-T(E_F)/T(*CNP*). Since the background IR extinction was all cancelled out, the peaks in the as-obtained extinction spectrum were resulted from the plasmon resonances which were strongly dependent on the electronic properties of the graphene.

Electrical Characteristics

Gate voltage-dependent resistance properties of the graphene devices were detected by applying a top gate and a back gate, respectively, as shown in Figure 1c. The CNP appears at 98 V by sweeping the back-gate voltage from -100 to 100 V (blue carve) while it appears at 0.53 V in the transfer characteristics of the same graphene sample with an ion-gel top-gate (red carve). The device was found to be a typical ambipolar FET as manifested by the 'V' shape of the resistance dependence on the gate voltage. The graphene at zero gate voltage was found to be highly p-type doped. This can be attributed to the absorption of impurities (e.g. water molecules) [40] and the effect of surface dangling bonds of the SiO_2 substrate.[41,42] In addition, the maximum resistivity was found to increase after the ion-gel was spin coated. This phenomenon likely originated from the additional impurities introduced into the graphene by ion-gel.[35]

From the determined transfer characteristics, and capacitance and thickness of the dielectric, we calculated the carrier concentration and E_F of the graphene using a standard parallel plate capacitor model (see details below). For the SiO_2 thin film, using a relative dielectric constant of 3.9 and a thickness of 300 nm, the capacitance was calculated as 0.0121 μFcm^{-2}.[15] The capacitance of the ion-gel dielectric was calculated as 2.42 μFcm^{-2} from a relationship that the shift in the back-gate voltage at CNP ($V_{bg,\,CNP}$) is linearly dependent on the change of applied top-gate voltage (V_{tg}) and $\frac{C_{tg}}{C_{bg}} = -\frac{\Delta V_{bg,CNP}}{\Delta V_{tg}}$ (see Figure S3 in Supplementary Information). Based on the value of capacitance, the dielectric constant of ion-gel can be calculated by using the conventional capacitance equation, $C = \frac{\varepsilon}{4\pi\kappa t}$, where κ is the static dielectric constant and t is the thickness of the Debye layer. Assuming a Debye length of 2 nm,[30] we obtained the dielectric constant as 5.5 for the ion-gel composed of $LiClO_4$ and PEO, which is consistent with previous reported values of PEO (~5).[43]

For both top-gated and back-gated graphene FET, the dependence of the carrier density on the gate voltage satisfies the equation:[26,27,35]

$$V_g - V_{CNP} = \frac{\hbar|\nu_F|\sqrt{\pi n}}{e} + \frac{ne}{C_g},$$

where V_g is the gate voltage, V_{CNP} is the charge neutrality point voltage, ν_F =1.1×10^6 m/s is the Fermi velocity,[44] n is the carrier density and C_g is the capacitance of gate dielectric. Combined with the relation between E_F and the carrier density of graphene $E_F = \hbar|\nu_F|\sqrt{\pi n}$, we obtained the relation between E_F and the gate voltages (see Supplementary Information). As shown in Figure 1d, E_F is plotted as a function of both the ion-gel top-gate voltage (V_{tg}) and the SiO_2 back-gate voltage (V_{bg}). When the V_{tg} is tuned from -4 to 4 V, the values of E_F shifts from about -0.94 to 0.81 eV. This shift of E_F is much larger than the change made by back gate, which is from about -0.5 to 0.05 eV with V_{bg} shifted from -100 to 100 V.

Plasmon Resonance Frequencies Characteristics

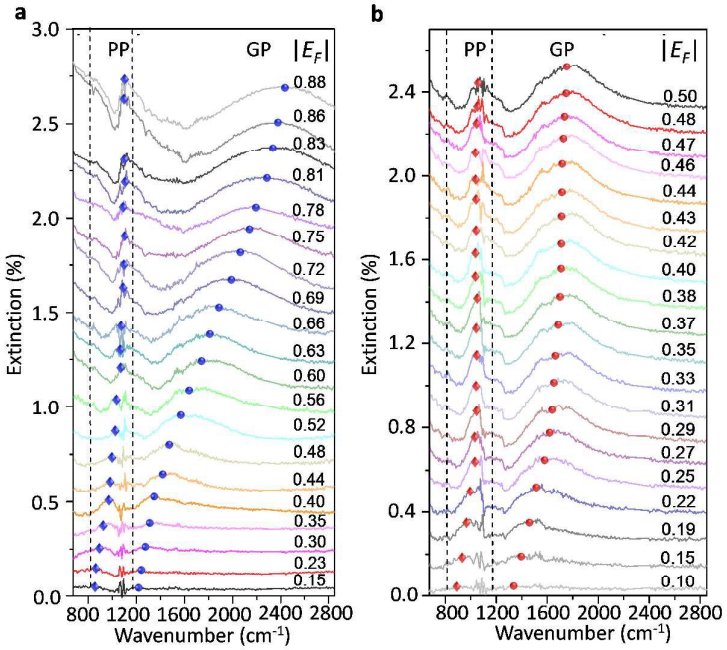

Figure 2. (a) Extinction spectra (T=*1*-T(E_F)/T(*CNP*)) of the graphene nanoribbon array at various values of E_F controlled by the ion-gel top gate. (b) Extinction spectra of the same device at various E_F values controlled by the back gate. These spectra were characterized before the ion-gel film was coated on the device. The absorption peaks of CO_2 (ranging from 2244 to 2395 cm^{-1}) in the ambient air were replaced by straight lines.

The plasmonic properties of as-prepared low voltage-controlled and broadly tunable mid-infrared graphene devices were experimentally characterized for performance. Because the electrical tunability of graphene is symmetric with respect to the CNP, we focused on the hole-doping regime for simplicity. Figure 2a shows the extinction spectra of the graphene nanoribbon array at different E_F controlled by the ion-gel top gate. The extinction spectra of the same graphene nanoribbon array at different E_F controlled by the SiO_2 back gate are used for comparison (Figure 2b). In both the top-gated and back-gated strategies, there are two distinct resonance peaks in the extinction spectra, as indicated by diamonds and spheres in Figures 2a and 2b. These peaks are ascribed to the coupling of graphene plasmon to two surface optical (SO) phonons of SiO_2 at 806 cm^{-1} (ω_{sp1}) and 1168 cm^{-1} (ω_{sp2}), respectively.[45,46] In order to better compare the electrical tunability of graphene plasmons controlled by the ion-gel and SiO_2, we used narrow graphene ribbons (~65 nm) to reduce this obvious plasmon-phonon coupling by shifting the pristine plasmon resonance frequency of graphene to energies much higher than ω_{sp2}. In most of these extinction spectra (except for the condition at low Fermi levels), the first resonance peaks (diamonds) are phonon-like polaritons (PP) and the second ones (spheres) are graphene plasmon-like polaritons (GP), which are the main peaks in the extinction spectra.

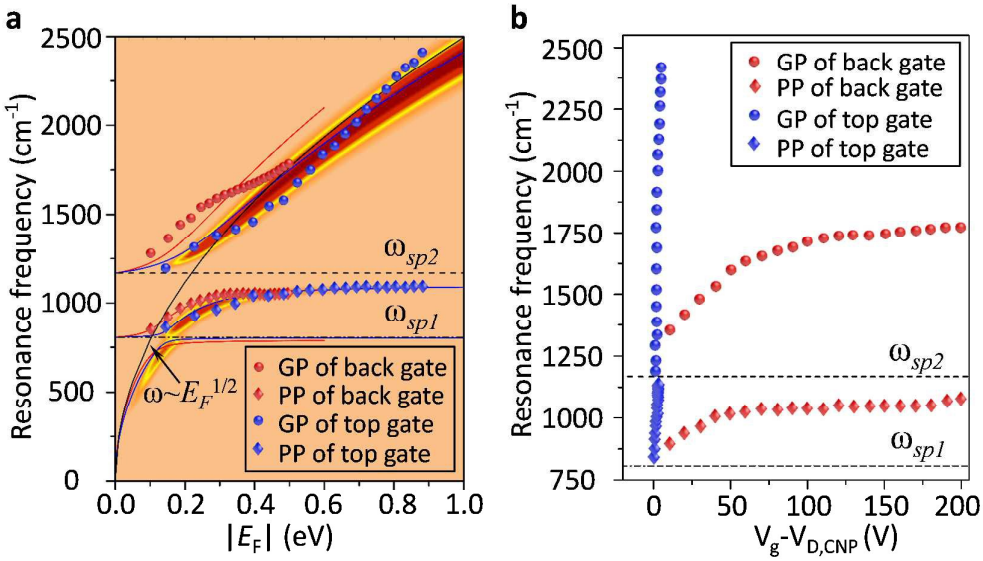

Figure 3. (a) The calculated resonance frequencies of PP and GP peaks as a function of E_F controlled by the top gate (blue curves) and the back gate (red curves), respectively. The two-dimensional pseudo-colour background is calculated from the loss function of graphene plasmons controlled by the ion-gel top gate. The experimental data of PP (diamonds) and GP (spheres) peaks extracted from Figure 2a and 2b are also plotted. (b) The dependence of the resonance frequencies of PP and GP peaks on the voltage of V_{tg} and V_{bg} shifted from the corresponding CNP, respectively. Two SO phonons of SiO_2 are indicated by dashed lines.

The resonance frequency ω_{pl} for pristine graphene plasmons is determined by E_F and the wave vector q via the equation $\omega_{pl} = \sqrt{e^2 E_F q / (2\pi\hbar^2 \varepsilon_0 \varepsilon_r)}$,[7,19,47] where q=π/W. When q is fixed, the corresponding value of ω_{pl} scales as $E_F^{1/2}$. For the plasmon-phonon coupling system, when E_F of graphene increases, both the PP and the GP peaks gain intensity and shift to higher frequencies, as shown in Figure 2. The plasmon resonance frequencies of the graphene device controlled by the ion-gel top gate are lower than those of the same device at the same E_F controlled by the SiO_2 back gate (see Supplementary Information Figure S4). This is due to different effective dielectric environments of graphene for these two cases as the environment determines the plasmon resonance frequencies via $\omega \propto \varepsilon^{-1/2}$. For the SiO_2 back gate system (air/graphene/SiO_2), the average dielectric environment $\varepsilon_r = \frac{1}{2}(\varepsilon_{SiO2} + \varepsilon_{air})$=2.45, while for ion-gel top gate system (ion-gel/graphene/SiO_2), $\varepsilon_r = \frac{1}{2}(\varepsilon_{SiO_2} + \varepsilon_{ion-gel})$ = 4.67.

We used a generalized random phase approximation (RPA) theory to calculate the relationship between E_F and the graphene plasmon resonance frequency in the condition of

plasmon-phonon coupling.[45,48-50] Calculations were performed according to Yang, *et al.*[33] Figure 3a shows the calculated results for a graphene nanoribbon with 65 nm ribbon width at varying E_F as controlled by both the ion-gel dielectric top gate (blue lines) and the SiO_2 back gate (red lines) alongside experimental data (diamonds and spheres) extracted from the extinction spectra of Figures 2a and 2b. The two-dimensional pseudo-colour background was calculated from the loss function of the graphene plasmons controlled with the ion-gel dielectric top gate. The simulation results are in excellent agreement with our experimental results. The used Fröhlich-like coupling strength between plasmons and two SO phonons of SiO_2 are represented in Figure S5 (for the ion-gel top gate and for the SiO_2 back gate). Small deviation between experimental and theoretical values mainly originates from the effect of the phonon-photon coupling of the SiO_2 substrate and the calculation error of the ion-gel dielectric constant.

The plasmon resonance frequencies were plotted as a function of gate voltage shifted from CNP for both SiO_2 back gate (red) and ion-gel top gate (blue), respectively (Figure 3b). The GP peak dramatically shifts from 1184 to 2455 cm^{-1} ($\Delta\omega$=1271 cm^{-1}) and the PP peak shifts from 842 to 1119 cm^{-1} ($\Delta\omega$=277 cm^{-1}) by adjusting V_{tg} to shift 4 V from CNP. In contrast, the GP peak shifts from 1374 to 1753 cm^{-1} ($\Delta\omega$=379 cm^{-1}) and the PP peak shifts from 906 to 1065 cm^{-1} ($\Delta\omega$=157 cm^{-1}) when V_{bg} shifts 200 V from CNP. The obtained shift of the GP peak by ion-gel top gate is nearly 3.5 times as much as the value obtained by SiO_2 back gate while the applied voltage is just 1/50th of the latter.

Plasmon-phonon Coupling Between Graphene and Ion-gel

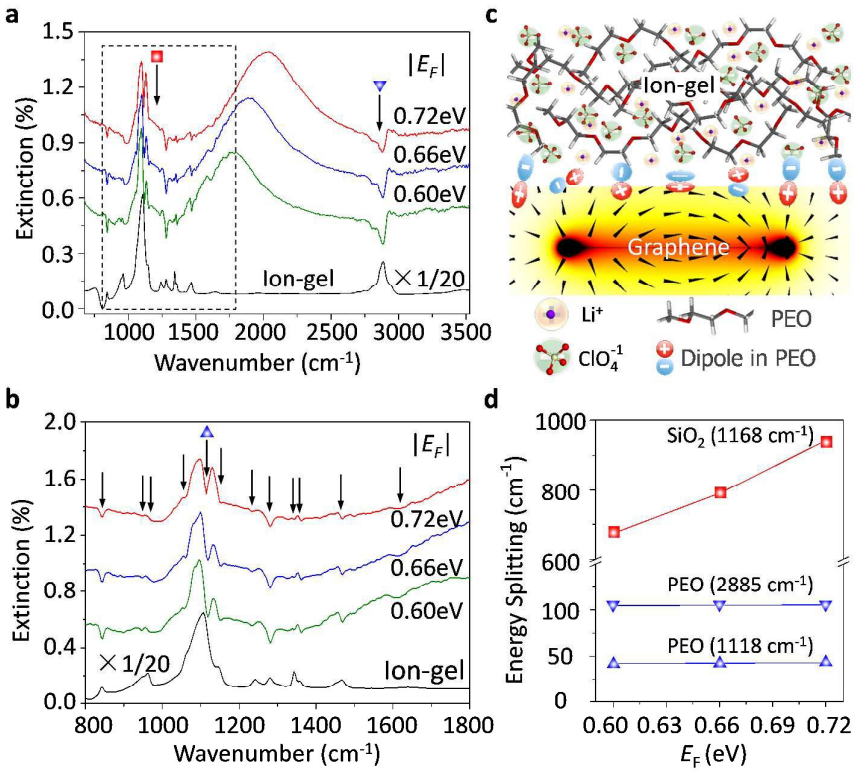

Figure 4. (a) Three selected extinction spectra of graphene nanoribbon array at different E_F controlled by ion-gel top gate with enlarged view. The infrared extinction spectrum of the ion-gel film is shown for comparison. The arrow under red square indicates the SO phonon of SiO_2 at 1168 cm^{-1}. The arrow under the blue triangle indicates the molecular resonance of PEO at 2885 cm^{-1}. (b) The zoom-in spectra of Figure 4(a) illustrating the coupling between graphene plasmons and the dipole moments of C-O-C stretching vibration of PEO molecules. The arrows indicate the IR active molecular resonances of PEO. (c) Schematic of coupling mechanism of graphene plasmons and PEO optical phonons. (d) Dependence of energy splitting induced by plasmon-phonon coupling on Fermi levels. For graphene/PEO case, the deepest dips at 1118 (blue triangles, up) and 2885 cm^{-1} (blue triangles, down) are selected as instances.

Graphene plasmons in the mid-infrared spectral range can interact strongly with phonons of surrounding dielectrics, such as the SO phonons of SiO_2 and the optical phonons of *h*-BN.[33,51] These strong plasmon-phonon couplings impede the electrostatic tunability of graphene plasmon significantly, especially at around the phonon energies. Thus, to explore how the ion-gel phonons affect graphene plasmons is of great importance. As shown in Figure 4a, the molecular vibration modes of the ion-gel can also interact with the graphene plasmon mode. However, the resulting shape is completely

different from the case when SiO_2 phonons are coupling with graphene plasmons. The SiO_2 phonons split the plasmon resonance peak into well separated multi-peaks (The PP peaks and the GP peaks), while ion-gel only introduce several shallow dips appearing in the extinction spectra (Figure 4a). The most obvious dips at 844, 1118, 1280 and 2885 cm^{-1} are accompanied with other dips at 946, 974, 1061, 1154, 1233, 1344, 1363, 1469, and 1610 cm^{-1}. These dips correspond to the respective IR group vibrations of PEO based on comparison to the IR absorption peaks of the ion-gel thin film. In order to exhibit these plasmon-phonon coupling signals more clearly, zoom-in spectra of Figure 4a in the range from 1000 to 1500 cm^{-1} (between the two dashed lines) are shown in Figure 4b. The strong C-O-C stretching mode at ~1118 cm^{-1} of PEO molecules couples with graphene plasmon and slightly splits the PP peak.

When the plasmon mode interacts with a phonon mode, the coupling of external light to the phonon mode (*i.e.* phonon absorption) can be significantly enhanced due to the plasmon excitation via the near field enhancement.[13] The induced phonon resonances form polariton waves with an opposite phase with respect to the plasmon polaritons (Figure 4c). These two waves with the same wavelength and opposite phase cause coherent destructive interference between them, which results in dips in the plasmon resonance extinction peaks. According to the interference theory of waves, the shape of the dips is mainly determined by the intensity of the induced phonon polariton waves, which determined the coupling strengths. For the plasmon-phonon polaritons, the coupling strength is proportional to the energy splitting of the dip.[52] Figure 4d presents the dependence of the energy splitting on Fermi levels for both graphene/PEO and graphene/SiO_2 systems. For both cases, the coupling strength increases coinciding with the shift of Fermi level, that is, the increasing electromagnetic field strength of graphene plasmon. For graphene/PEO system, the coupling strength is much less than that of graphene/SiO_2. The latter enters a strong coupling regime as the splitting energies are much larger than the sum of linewidths of graphene plasmon and SiO_2 phonon. The former is a weak coupling system as the splitting energy is much less than the sum of the linewidths of graphene plasmon and the phonon resonance. This is because the densities of phonon modes in the ion-gel are much smaller than those in the SiO_2 films due to a disordered arrangement of long PEO molecular chains (Figure 4c), which is consistent with the coupling between plasmon and other molecular vibrations.[53] Thus, compared with conventional oxide dielectric materials, ion-gel dielectric has very limited perturbation on the properties of graphene plasmon.

Plasmon Lifetime Characteristics

The influence of the ion-gel dielectric on plasmon lifetimes, which is closely related to the plasmonic performance, was also studied. The plasmon lifetimes T can be obtained via $T=2\hbar/\Gamma$ for the far field extinction spectra,[33,54] where Γ is the linewidths of resonance peaks extracted by using Fano curve fitting (See Supplementary Materials and Figure S6a). We compared the graphene plasmon lifetimes of the graphene/SiO_2 device before and after spin coated with the ion-gel top gate by plotting the lifetimes of the GP mode as a function of resonance frequencies (Figure S6b). In both systems, the lifetimes dramatically decreased as the resonance frequencies increased. The lifetimes increased slightly at the same resonance frequency after adding the ion-gel film. This is because the ion-gel coating introduces additional scattering (such as charged impurities) to the graphene plasmons. The condition is very similar to that of free standing graphene transferred onto supporting substrates, whose carrier mobility decreases dramatically due to introduced phonon scattering and charged impurity scattering. However, the mobility of graphene is less reduced by ion gel for its weak phonon scattering.

Conclusions

In conclusion, we achieved a low voltage-controlled and broadly tunable graphene plasmonic device with a top gate prepared by the simple and convenient method of using a spin-coated ion-gel thin film as a dielectric. The ion-gel top gate can shift the plasmon resonance frequency to 1271 cm^{-1} which is nearly 3.5 times the value obtained by a SiO_2 back gate (379 cm^{-1}) while applying $1/50^{th}$ of the voltage shifted from CNP (*e.g.* 4 V compared to the 200 V required for a SiO_2 back gate). In addition, unlike the graphene plasmon resonance peaks being split by the SO phonon of SiO_2 and the optical phonons of *h*-BN, the coupling between a graphene plasmon and phonons of PEO is much weaker and has very limited effects on the plasmonic properties . On the whole, the ion-gel is an excellent dielectric for broadly tunable graphene plasmon devices.

Experimental Section

The device consists of a graphene sheet prepared by chemical vapor deposition (CVD) on copper foil which was transferred to a SiO_2 (300 nm)/Si substrate. The sample was identified to be a monolayer by micro-Raman microscope (Horiba JobinYvon, LabRAM HR800) before processing. The nanoribbon arrays were patterned using electron-beam lithography on graphene which was then etched away using oxygen plasma. The graphene nanoribbons were characterized by atomic force microscopy (s-SNOM, Neaspec) using tapping mode and SEM (Hitachi, S-4800). The source, drain and top gate electrode of the device were made by e-beam lithography, followed by e-beam evaporation of 100 nm of gold and subsequent lift-off in acetone. The ion-gel dielectric material was achieved by dissolving polyethylene oxide (PEO) and $LiClO_4$ in methanol with a mass ratio of 1:0.12:40, as reported in previous work.[27,35] The compounded ion-liquid is then spun onto a graphene transistor at 5000 RPM, followed by baking at 60°C to remove any residual methanol. The electrical transport properties were characterized with a semiconductor

parameter analyzer (Agilent, 4294A). The V_{tg} was applied by inserting a wolframium electrode within the polymer layer. The measurement set-up for the device consisted of an infrared microscope coupled to a Fourier-transform infrared spectrometer (ThermoFisher, Nicolet iN10), used in conjunction with a power source (Keithley 2612B). All the measurements were performed at room temperature and under ambient atmosphere. The finite element method was used to simulate the plasmonic responses of the devices.

Acknowledgements

This work is supported by the National Basic Research Program of China (Grant No.2015CB932400), the National Natural Science Foundation of China (Grant No.51372045, and No. 11174252) and the Bureau of International Cooperation, Chinese Academy of Sciences (121D11KYSB20130013).

Notes and references

1 Q. Bao and K. P. Loh, *ACS Nano*, 2012, **6**, 3677.
2 T. Stauber, J. *Phys.: Condens. Matter*, 2014, **26**, 123201.
3 F. MinovKoppensich, D. Chang, S. Thongrattanasiri and F. García de Abajo, *Optics and Photonics News*, 2011, 22, 36.
4 T. Low and P. Avouris, *Acs Nano*, 2014, **8**, 1086.
5 X. Luo, T. Qiu, W. Lu and Z. Ni, *Mater. Sci. Eng. R-Rep*, 2013, **74**, 351.
6 M. Jablan, M. Soljacic and H. Buljan, *Proc. IEEE*, 2013, **101**, 1689.
7 A. Grigorenko, M. Polini and K. Novoselov, *Nature Photon.,* 2012, **6**, 749.
8 F. J. Garcia de Abajo, *Acs Photon.*, 2014, **1**, 135.
9 F. Bonaccorso, Z. Sun, T. Hasan and A. Ferrari, *Nature Photon.*, 2010, **4**, 611.
10 B. Sensale-Rodriguez, R. Yan, M. M. Kelly, T. Fang, K. Tahy, W. S. Hwang, D. Jena, L. Liu and H. G. Xing, *Nature Commun.*, 2012, **3**, 780.
11 S. Badhwar, R. Puddy, P. R. Kidambi, J. Sibik, A. Brewer, J. R. Freeman, H. E. Beere, S. Hofmann, J. A. Zeitler and D. Ritchie, *IEEE Photonics J.*, 2012, **4**, 1776.
12 L. Ju, B. Geng, J. Horng, C. Girit, M. Martin, Z. Hao, H. A. Bechtel, X. Liang, A. Zettl, Y. R. Shen and and F. Wang, *Nature Nanotech.*, 2011, **6**, 630.
13 H. Yan, X. Li, B. Chandra, G. Tulevski, Y. Wu, M. Freitag, W. Zhu, P. Avouris and F. Xia, *Nature Nanotech.*, 2012, **7**, 330.
14 L. Vicarelli, M. Vitiello, D. Coquillat, A. Lombardo, A. Ferrari, W. Knap, M. Polini, V. Pellegrini and A. Tredicucci, *Nature Mater.*, 2012, **11**, 865.
15 H. Xu, Z. Zhang, H. Xu, Z. Wang, S. Wang and L.-M. Peng, *ACS Nano*, 2011, ***5***, 5031.
16 K. S. Novoselov, A. K. Geim, S. Morozov, D. Jiang, Y. Zhang, S. a. Dubonos, I. Grigorieva and A. Firsov, *Science*, 2004, ***306***, 666.
17 A. K. Geim and K. S. Novoselov, *Nature Mater.*, 2007, 6, 183.
18 J. Liu, Q. Qian, Y. Zou, G. Li, Y. Jin, K. Jiang, S. Fan and Q. Li, *Carbon*, 2014, ***68***, 480.
19 S. Badhwar, J. Sibik, P. R. Kidambi, H. E. Beere, J. A. Zeitler, S. Hofmann and D. A. Ritchie, *Appl. Phys. Lett.*, 2013, ***103***, 121110.
20 Y. Zhang, T.-T. Tang, C. Girit, Z. Hao, M. C. Martin, A. Zettl, M. F. Crommie, Y. R. Shen and F. Wang, *Nature*, 2009, ***459***, 820.
21 K. Zou, X. Hong, D. Keefer and J. Zhu, *Phys. Rev. Lett.*, 2010, ***105***, 126601.
22 A. Konar, T. Fang and D. Jena, *Phys. Rev. B*, 2010, ***82***, 115452.
23 L. Liao, J. Bai, Y. C. Lin, Y. Qu, Y. Huang and X. Duan, *Adv. Mater.*, 2010, ***22***, 1941.
24 S. Kim, J. Nah, I. Jo, D. Shahrjerdi, L. Colombo, Z. Yao, E. Tutuc and S. K. Banerjee, *Appl. Phys. Lett.*, 2009, ***94***, 062107.
25 J. Bai, L. Liao, H. Zhou, R. Cheng, L. Liu, Y. Huang and X. Duan, *Nano Lett.*, 2011, ***11***, 2555.
26 B. Chakraborty, A. Das and A. Sood, *Nanotechnology*, 2009, ***20***, 365203.
27 J. Liu, Q. Li, Y. Zou, Q. Qian, Y. Jin, G. Li, K. Jiang and S. Fan, *Nano Lett.*, 2013, ***13***, 6170.
28 M. A. B. H. Susan, T. Kaneko, A. Noda and M. Watanabe, *J. Am. Chem. Soc.*, 2005, ***127***, 4976.
29 S.-K. Lee, S. H. Kabir, B. K. Sharma, B. J. Kim, J. H. Cho and J.-H. Ahn, *Nanotechnology*, 2014, ***25***, 014002.
30 J. H. Cho, J. Lee, Y. Xia, B. Kim, Y. He, M. J. Renn, T. P. Lodge and C. D. Frisbie, *Nature Mater.*, 2008, ***7***, 900.
31 N. K. Emani, T.-F. Chung, A. V. Kildishev, V. M. Shalaev, Y. P. Chen and A. Boltasseva, *Nano Lett.*, 2013, ***14***, 78.
32 Z. Fang, S. Thongrattanasiri, A. Schlather, Z. Liu, L. Ma, Y. Wang, P. M. Ajayan, P. Nordlander, N. J. Halas and F. J. García de Abajo, *ACS Nano*, 2013, ***7***, 2388.
33 X. Yang, F. Zhai, B. Bai, H. Hu, J. Chen and Q. Dai, *arXiv preprint arXiv:1504.00195*, 2015.
34 A. Pachoud, M. Jaiswal, P. K. Ang, K. P. Loh and B. Oezyilmaz, *EPL-Europhys Lett.*, 2010, ***92***, 27001.
35 A. Das, S. Pisana, B. Chakraborty, S. Piscanec, S. Saha, U. Waghmare, K. Novoselov, H. Krishnamurthy, A. Geim and A. Ferrari, *Nature Nanotech.*, 2008, ***3***, 210.
36 B. J. Kim, H. Jang, S.-K. Lee, B. H. Hong, J.-H. Ahn and J. H. Cho, *Nano Lett.*, 2010, ***10***, 3464.
37 J. Ye, M. F. Craciun, M. Koshino, S. Russo, S. Inoue, H. Yuan, H. Shimotani, A. F. Morpurgo and Y. Iwasa, *Proc. Natl. Acad. Sci. U.S.A.*, 2011, **108**, 13002.
38 X. He, N. Tang, L. Gao, J. Duan, Y. Zhang, F. Lu, F. Xu, X. Wang, X. Yang and W. Ge, *Appl. Phys. Lett.*, 2014, ***104***, 143102.
39 J. Lee, M. J. Panzer, Y. He, T. P. Lodge and C. D. Frisbie, *J. Am. Chem. Soc.*, 2007, ***129***, 4532.
40 J. Kong, N. R. Franklin, C. Zhou, M. G. Chapline, S. Peng, K. Cho and H. Dai, *Science*, 2000, **287**, 622.
41 Y. Shi, X. Dong, P. Chen, J. Wang and L.-J. Li, *Phys. Rev. B*, 2009, **79**, 115402.
42 T. O. Wehling, M. I. Katsnelson and A. I. Lichtenstein, *Appl. Phys. Lett.*, 2008, **93**, 202110.
43 R. H. Boyd, *J. Polym. Sci., Polym. Phys. Ed.*, 1983, **21**, 505.
44 C. Hwang, D. A. Siegel, S.-K. Mo, W. Regan, A. Ismach, Y. Zhang, A. Zettl and A. Lanzara, *Sci. Rep.*, 2012, **2**, 590.
45 H. Yan, T. Low, W. Zhu, Y. Wu, M. Freitag, X. Li, F. Guinea, P. Avouris and F. Xia, *Nature Photon.*, 2013, **7**, 394.
46 X. Yang, X. T. Kong, B. Bai, Z. Li, H. Hu, X. Qiu and Q. Dai, *Small*, 2015, **11**, 591.
47 S. H. Abedinpour, G. Vignale, A. Principi, M. Polini, W.-K. Tse and A. MacDonald, *Phys. Rev. B*, 2011, **84**, 045429.
48 E. Hwang, R. Sensarma and S. D. Sarma, *Phys. Rev. B,* 2010, **82**, 195406.
49 M. Jablan, M. Soljačić and H. Buljan, *Phys. Rev. B*, 2011, **83**, 161409.
50 E. Hwang and S. D. Sarma, *Phys. Rev. B*, 2007, **75**, 205418.
51 V. W. Brar, M. S. Jang, M. Sherrott, S. Kim, J. J. Lopez, L. B. Kim, M. Choi and H. Atwater, *Nano Lett.*, 2014, **14**, 3876.
52 Y. Jia, H. Zhao, Q. Guo, X. Wang, H. Wang and F. Xia, ACS Photonics, 2015, **2**, 907.
53 F. Neubrech, A. Pucci, T. W. Cornelius, S. Karim, A. García-Etxarri and J. Aizpurua, *Phys. Rev. Lett.*, 2008, **101**, 157403.
54 C. Sonnichsen, T. Franzl, T. Wilk, G. von Plessen, J. Feldmann, O. Wilson and P. Mulvaney, *Phys. Rev. Lett.*, 2002, **88**, 077402.